Changes in Sahelian annual vegetation growth and phenology since 1960: A modeling approach

C. Pierre, M. Grippa, E. Mougin, F. Guichard, L. Kergoat

PII: S0921-8181(15)30157-0
DOI: doi: 10.1016/j.gloplacha.2016.06.009
Reference: GLOBAL 2437

To appear in: *Global and Planetary Change*

Received date: 14 December 2015
Revised date: 14 June 2016
Accepted date: 17 June 2016

Please cite this article as: Pierre, C., Grippa, M., Mougin, E., Guichard, F., Kergoat, L., Changes in Sahelian annual vegetation growth and phenology since 1960: A modeling approach, *Global and Planetary Change* (2016), doi: 10.1016/j.gloplacha.2016.06.009

Changes in Sahelian annual vegetation growth and phenology since 1960: a modeling approach

C. Pierre[1,2], M. Grippa[1], E. Mougin[1], F. Guichard[3], L. Kergoat[1]

[1] Géosciences Environnement Toulouse (GET)

Université de Toulouse, UMR CNRS 5563, IRD UR 234

16 Avenue Edouard Belin, 31400 Toulouse, France

manuela.grippa@get.obs-mip.fr

laurent.kergoat@get.obs-mip.fr

eric.mougin@get.obs-mip.fr

[2] Laboratoire Interuniversitaire des Systèmes Atmosphériques (LISA)

Universités Paris Est Créteil & Paris Diderot, UMR CNRS 7583

61 Avenue du Général de Gaulle, 94000 Créteil, France

caroline.pierre@lisa.u-pec.fr (corresponding author, phone number: +33 1 45 17 15 79)

[3] Centre Nationale de Recherches Météorologiques (CNRM)

Meteo-France & UMR CNRS 3589

42 Avenue Gaspard Coriolis, 31100 Toulouse, France

francoise.guichard@gmail.com

Abstract

In semi-arid areas like the Sahel, vegetation is particularly sensitive to climate variability and can play an important role in surface-atmosphere coupling. After a wet period extending from 1950 to 1970, the Sahel experienced a severe drought in the 1970s and 1980s, followed by a partial recovery of rainfall and a "re-greening" of vegetation beginning in the 1990s. This study explores how the multidecadal variability of Sahelian rainfall and particularly the drought period have affected vegetation phenology and growth since 1960.

The STEP model, which is specifically designed to simulate the Sahelian annual vegetation, including the dry season processes, is run over an area extending from 13°N to 18°N and from 20°W to 20°E. Mean values, interannual variability and phenological characteristics of the Sahelian annual grasslands simulated by STEP are in good agreement with MODIS derived production and phenology over the 2001-2014 period, which demonstrates the skill of the model and allows the analysis of vegetation changes and variability over the last 50 years.

It was found that droughts in the 1970s and 1980s shortened the mean vegetation cycle and reduced its amplitude and that, despite the rainfall recovery since the 1990s, the current conditions for green and dry vegetation are still below pre-drought conditions. While the decrease in vegetation production has been largely homogeneous during droughts, vegetation recovery has been heterogeneous over the Sahel since 1990, with specific changes near the western coast and at the eastern edge of the West African monsoon area. Since 1970, the Sahel also experienced an increased interannual variability in vegetation mass and phenology. In terms of phenology, region-averaged End and Length of Season are the most variable, while maximum date and Start of Season are the least variable, although the latter displays a high variability locally.

Keywords

Vegetation, Sahel, modeling, phenology, droughts

Highlights

Sahelian annual vegetation is simulated from 1960 to 2014

Simulated vegetation captures phenology and spatial patterns as observed by satellite

The present vegetation cover is still far below its pre-drought levels

1. Introduction

The strongest multidecadal drought of the 20th century occurred in the West African Sahel. After a wet period extending from 1950 to 1969, the rainfall series exhibited a marked break (*L'Hôte et al.,* 2002) with extreme droughts in the 1970s and 1980s (*Ozer et al.,* 2003; *Nicholson et al.,* 1998). Since the early 1990s, the Sahel has been experiencing a rain recovery, occurring contrastingly in western, central and eastern parts of the area (*Lebel and Ali,* 2009). At the same time, a positive trend and a high interannual variability of the Sahelian vegetation greenness have been observed from satellite-based vegetation indices (e.g. *Olsson et al*., 2003; *Anyamba and Tucker*, 2005; *Philippon et al.,* 2007; *Fensholt et al.,* 2009; *Dardel et al.,* 2014a; *Meroni et al.,* 2014). This "re-greening" of the Sahel is primarily driven by rainfall (*Lotsch et al.,* 2003*; Hickler et al.,* 2005; *Dardel et al.,* 2014b), but also possibly by human activities such as local projects facilitating the regeneration of natural vegetation (*Herrmann et al.,* 2005).

In semi-arid areas, vegetation growth is controlled primarily by water availability (*Lieth*, 1975; *Hickler et al.,* 2005; *Herrmann et al.,* 2005), although biogeochemical factors (e.g. nutrient availability, soil types, vegetation types) and/or anthropogenic factors (cropping, grazing, fire regime) also play an important role. Yet, several questions are still under debate due to the scarcity of long-term datasets. Among unsettled questions is the relationship between plant production and rainfall amount, and its evolution in the long term (*Le Houerou et al.*, 1988; *Prince et al*., 1998, 2007; *Diouf and Lambin*, 2001; *Hein and de Ridder*, 2006; *Huber et al.*, 2011; *Ruppert et al.*, 2012; *Dardel et al.*, 2014b), as well as the role and the evolution of intraseasonal variability in occurrences such as dry spells, start dates of the rainy season, and extreme events (*Diouf and Lambin*, 2001; *Ruppert et al.*, 2012; *Bobée et al*., 2012). Most studies of the Sahel are limited to the period from 1980 to the present, which leaves mostly unanswered the question of the vegetation 'recovery' compared to pre-drought conditions, as well as its spatial extent. Whether there has been, on the whole, a degradation or resilience of Sahelian ecosystems over this longer time period is still unknown.

In addition to trends in annual production or greenness, the Sahelian vegetation phenology has been specifically scrutinized as it is a good gauge of plant response to climate and anthropogenic changes. Analyzing satellite-based Normalized Difference Vegetation Indices (NDVI) over 1982-2005, *Heumann et al.* (2007) reported two different types of greening: an increase of the amplitude of the vegetation's annual cycle in the Sahel, and an increase of the length of the vegetation cycle in the Soudanian and Guinean area. Following a similar methodology, *Butt et al.* (2011) observed a high latitudinal variability of phenological

characteristics over southern Mali from 2000 to 2010. Whether these features are valid over a longer time scale is unknown.

More generally, a good understanding of the Sahelian vegetation dynamics is necessary to answer several scientific questions. Annual production is a key variable for natural resources and ecosystems services, and for desertification issues (see for instance references reviewed by *Dardel et al.*, 2014a, and *Karlson and Ostwald*, 2016). Annual Sahelian grass is a key resource for pastoralism, particularly during the dry season. The annual vegetation cycle and its variability is also known to impact surface-atmosphere interaction through the energy and water balance (*Zeng et al.*, 1999; *Cayrol et al.*, 2000; *Samain et al.*, 2008; *Timouk et al.*, 2009, among others). Finally, dry season soil protection via vegetation is important for wind erosion control and Sahelian dust emissions (*Sterk, 2003*) and surface radiation budget (*Samain et al.*, 2008, *Vamborg et al.*, 2011).

Earlier global vegetation models were shown to simulate the vegetation phenology (i.e. the periodic plant life events and their evolution) in West Africa rather poorly (*Bondeau et al.*, 1999), but attempts have been made to improve phenology modeling in semi-arid areas (*Ciret et al.*, 1999; *Jolly and Running*, 2004; *Brender et al.*, 2011; *Berg et al.*, 2011; *Traore et al.*, 2014) or globally, with a close-up on the Sahel (*Gibelin et al.*, 2006). Specific models of plant phenology in the Tropics have also been developed from ground-based surveys, but most of these studies focused on woody or perennial plants (e.g. *Archibald and Scholes*, 2007; *Choler et al.*, 2011).

The objective of this study is to investigate how the multidecadal variability of Sahelian rainfall and the droughts of the 1970s and 1980s have affected vegetation production and phenology. Given that satellite observations started mostly in the 1980s, models must consider the wet period before the drought at a regional and pluriannual scale. The Sahelian Transpiration, Evaporation and Productivity (STEP) model, specifically designed to represent Sahelian annual grasses, is used for that purpose.

First, the STEP model's ability to capture the main phenological characteristics (spatial and interannual variability, length and amplitude of the vegetation cycle) of the Sahelian herbaceous vegetation over the current period (2001-2014) is analyzed. Indeed, spectral indices are well suited to characterizing vegetation phenology, and they are widely used for that purpose (e.g. *Moulin et al.*, 1997; *Zhang et al.*, 2003; among others). Model outputs have been compared to MODerate resolution Imaging Spectroradiometer (MODIS) satellite observations (section 3.1), which have been shown to match vegetation phenology measurements over two sites in Senegal (*Bobée et al.*, 2012). Then, vegetation changes since

1960, thus including a wet period before the Sahelian droughts, are investigated with a particular focus on vegetation phenology (start, length and end of the season), as well as dry season vegetation and the impact of grazing pressure, which have rarely been studied before now.

2. Materials and methods

2.1. MODIS data

The Nadir BRDF Adjusted Reflectance (NBAR) product (MCD43C4, collection 5, combining TERRA and AQUA observations, *Schaaf and Wang*, 2015), provides reflectances of MODIS bands 1 (620-670 nm: near infrared), 2 (841-876 nm: infrared), 6 (1628-1652 nm) and 7 (2105-2155 nm, both short waves infrared) at 0.05° and 8-day time resolution over the 2001-2014 period. Two vegetation indices are derived from these observations:

$$NDVI = \frac{B_2 - B_1}{B_2 + B_1} \quad (1)$$

$$STI = \frac{B_6}{B_7} \quad (2)$$

where STI is the Soil Tillage Index (*Guerschman et al.*, 2009).

NDVI is well known for its good representation of green vegetation (e.g. *Myneni et al.*, 1995; *Anyamba and Tucker*, 2005). It is commonly used to monitor plant phenology of different ecosystems, including Sahelian grasslands (*Heumann et al.*, 2007; *Butt et al.*, 2011). Moreover, the integral of NDVI has been shown to provide good estimates of Sahelian plant production (*Tucker et al.*, 1986; *Prince et al.*, 1991; *Mbow et al.*, 2013; *Dardel et al.*, 2014a). iNDVI denotes the 'small integral' (*Mbow et al.*, 2013), which is obtained by integrating NDVI above the dry-season value; it is used as a proxy for vegetation production over the entire growth period.

Dry-season vegetation, commonly referred to as non-photosynthetic vegetation (NPV), is receiving increasing attention due to its important role in the carbon cycle, residue management, soil erosion and fire risk assessment. The availability of short-wave infrared bands from MODIS has fostered the development of different techniques, either based on end-members (e.g. *Okin and Gu*, 2015) or specifically-designed indices (*Guerschman et al.*, 2009; *Daughtry et al*., 2015). STI has recently been shown to provide accurate estimates of dry vegetation mass and cover fraction in drylands (*Guerschman et al.*, 2009) and in the Sahel (*Jacques et al.*, 2014; *Kergoat et al.*, 2015).

These indices are aggregated at 0.25° for comparison to model outputs (see 2.2). Then, a running mean over 5 dates is computed, and grid cells where the annual cycle is low (NDVI amplitude lower than 0.02) are discarded for both NDVI and STI.

2.2. The STEP model

The STEP model (*Mougin et al.,* 1995) has been specifically designed to simulate the growth and senescence of Sahelian annual grass. Previous studies have demonstrated its good skill for local (*Tracol et al.,* 2006; *Jarlan et al.,* 2005; 2008) to regional vegetation modeling through comparison to ground-data and satellite-based indices (*Lo Seen et al*., 1995; *Frison et al.,* 1998; *Jarlan et al*., 2002; *Pierre et al.*, 2011).

The STEP model is based on two submodels describing the water budget and vegetation growth. The water module estimates soil evaporation (depending on the soil surface resistance) and plant transpiration following Penman Monteith's approach, runoff, drainage, and soil moisture. The latter is calculated with a tipping bucket approach using up to four soil layers (up to 3 m deep). Soil water content at field capacity and wilting point are derived as a function of soil texture. Seed germination is triggered by soil moisture of the upper soil layer, whereas leaf senescence is controlled by soil water content in the rooting zone.

Vegetation mass is calculated at a daily time step from a set of differential equations relating the different vegetation components (green, standing dry, and litter). Biomass increment results from photosynthesis, from which growth and maintenance respiration are subtracted, and tissue mortality. Photosynthesis depends on the fraction of Absorbed Photosynthetically Active Radiation (fAPAR), water stress, and temperature effect. At the end of the rainy season, senescence is triggered and results in a rapid conversion of biomass to standing straws.

Recent developments have added a detailed representation of the dry vegetation (straws and litter) dynamics, responding to meteorological and biotic factors, including grazing effects (*Delon et al.,* 2015; *Pierre et al.,* 2015). Grazing corresponds to the impact of domestic cattle on the herbaceous vegetation mass through fodder intake and trampling. The grazing is simulated for the dry vegetation; the net effect of grazing during the rainy season is neglected, since there is some compensation between intake, trampling, increased tillering and fertilization by livestock (*Hiernaux et al.,* 2009a). Part of the standing straws becomes litter because of trampling by livestock and climate factors, while some straws and litter disappear through fodder intake. Finally, litter is also buried by livestock trampling and is decomposed according to climate factors.

The STEP model runs at a daily time step and provides herbaceous dry matter mass (green, straws, and litter, with total vegetation mass being the sum of these three components), Leaf Area Index (LAI), fAPAR, and cover fraction.

2.3. Simulations

Simulations were performed on a 0.25° x 0.25° grid, from 13°N to 18°N and from 20°W to 20°E, over 6-year time-windows representative of the Sahelian wet, dry and intermediate periods, called P1 to P5 (details in *Table 1*). P2 and P3 include the years of extreme drought (1972-1973 and 1983-1984). The model is spun up over one year preceding each period (e.g. 1959 for P1) to estimate initial vegetation mass and soil moisture. STEP is run for all years in the 2000-2014 period (referred to as PV for 'validation period') in order to benefit from all MODIS observations used for evaluation.

The input variables are daily meteorological data (surface rainfall, solar radiation, air temperature, air relative humidity, and wind speed), soil texture with depth, and grazing pressure (*Table 1*). Since Sahelian rainfall is poorly simulated by global meteorological models (e.g. *Roehrig et al.,* 2013), spatially interpolated rain gauge measurements were retained for the 1960-1995 period. Given that the spatial coverage of gauges networks has become scarce since the late 1990s and that data distribution has also been reduced, satellite rainfall estimates are used from that point onwards. The TRMM3B42 product (3-hour, 0.25° x 0.25°) of the Tropical Rainfall Measuring Mission has been selected for the period 2000-2014 for its good skills and compatibility with Sahelian vegetation modeling (*Pierre et al.,* 2011). The other meteorological data was taken from the ECMWF (European Center for Medium-range Weather Forecast) Re-Analysis ERA-40 and ERA-Interim with a 3-hour sampling over a common 1° x 1° spatial grid. Given the non-negligible difference between the two reanalyses (particularly for wind and short wave radiation), ERA-40 is adjusted to ERA-Interim based on their values over the overlap period (1979-2001). The mean difference between ERA-40 and ERA-Interim has been estimated in each 1° grid cell and for each Day of Year from 1979 to 2001. Then, the 1-month running mean of this difference was computed and applied to ERA-40 variables (solar radiation, air temperature, relative humidity, and wind speed) as a correcting factor.

Table 1: Simulation set-up for the different time-windows.

Soil texture and thickness are taken from the HWSD (Harmonized World Soil Database, 5 min resolution; *Fischer et al.*, 2008), aggregated at 0.25° x 0.25°. The topsoil layer is 0.3 m thick, while the subsoil layer is 0.7 m thick in most cases, and does not exist for superficial soil units. All soil types in a given 0.25° grid cell are considered (without averaging), according to their proportions. Simulations are performed for each soil type, and the final output is the weighted average of all simulations in each grid cell. For grazing pressure, a constant value is taken for the whole study area. For each 6-year time-window, grazing pressure is adapted from *Dicko et al.* (2006), who used the FAO (Food and Agriculture Organization) data: from 3 TLU.km^{-2} in the 1960s to 12 TLU.km^{-2} in the 2000s (with TLU standing for Tropical Livestock Unit). An additional simulation (PV*, P5*) has been performed for the 2000s with the lowest grazing pressure (3 TLU.km^{-2}) to investigate the impact of the grazing pressure on vegetation. The remaining parameters, to which the simulated vegetation is less sensitive, and which are difficult to document at a regional scale (vegetation mass at germination, efficiency of energy conversion into dry matter, proportion of dicots and grasses, proportion of C3 and C4-plants, and root distribution in the soil) are set to constant values previously determined or calibrated on study sites in Mali, Senegal and Niger (*Mougin et al.*, 1995; *Tracol et al.*, 2006; *Hiernaux et al.*, 2009a). Given the relatively

Period	P1	P2	P3	P4	P5 (PV)	P5* (PV*)
Years	1960-1965	1970-1975	1980-1985	1990-1995	2002-2007 (PV, PV* : 2001-2014)	
Rainfall input	Krigged gauges data				TRMM3B42	
Other meteorological inputs	ERA-40		ERA-Interim			
Grazing pressure (TLU/km²)	3	5	6	9	12	3
Soil Texture	HWSD					

large size of the grid cells (0.25° x 0.25°), runoff is neglected.

2.4. Comparison criteria

First, model outputs are compared to satellite observations over the 2001-2014 period; then the different periods Pi are compared. The use of satellite-based indices to estimate simulation reliability requires the selection of the model outputs to be compared to. To investigate interannnual variability, the total vegetation mass at the date of the green vegetation maximum is taken as a proxy of above-ground plant production, and the total vegetation mass is averaged over the October-June period as a measure of the vegetation amount during the dry season. These two values are compared to the integral of NDVI (iNDVI) and to the mean value of STI over October-June, respectively. For all variables, regional-mean values are the mean over all grid cells of the continental study area.

When considering annual cycles, STI, which is linearly related to the grass mass up to about 250 $g.m^{-2}$ (*Kergoat et al.,* 2015), can be directly compared to the simulated total vegetation mass. However, for green vegetation phenology, the model metric linearly related to NDVI is fAPAR (e.g. *Fensholt et al.,* 2004); it is therefore used for the comparison. Anomalies are defined as the deviation from the regional-mean annual cycle averaged over the pluriannual period.

Correlations indicated in this study correspond to the linear Pearson correlation coefficient. Associated significance values correspond to the Student's t-test of the null hypothesis; if not specified, the significance level for computing the correlation coefficient is 0.01. The coefficient of variation (standard deviation divided by mean) of simulated vegetation mass is also used to document interannual variability.

Phenological dates derived from STEP are defined as follows: Start of Season (SOS) is defined as the first Day of Year (DoY) when simulated green vegetation mass exceeds 1 $g.m^{-2}$, End of Season (EOS) corresponds to the first DoY after the annual vegetation maximum (if greater than 1 $g.m^{-2}$) when green vegetation mass becomes nil, and the Length of Season (LOS) is the time span between SOS and EOS.

In addition to these key dates of the phenological cycle, the agreement between satellite data and green vegetation simulations is examined using a more sophisticated method based on a quantile-quantile comparison. A given quantile of NDVI, for instance 19%, gives a series of 14 DoY, one for each year (175, 189, 169, 176, 170, 187, 186, 172, 188, 176, 180, 173, 181, 191 in this example). The average DoY over the 14 years (DoY 180 in this case) is taken as a reference, so that the 19% NDVI quantile documents the variability of the NDVI around DoY

180. For years with an early (resp. delayed) development of vegetation, the 19% quantile will be reached earlier (resp. later). For the model equivalent metric (fAPAR), a similar approach is used, yielding a series that gives the same average DoY as the NDVI-derived DoY (in this case 180). Then, the correlation between the series obtained with NDVI and with fAPAR is analyzed. High correlation indicates that around DoY 180 (in this example), early (resp. late) years in NDVI correspond to early (resp. late) years in fAPAR, and that the two variables are consistent in terms of interannual variability around DoY 180. In practice, this computation is carried out every 10 days over the growing season (except at vegetation maximum, when this computation is precluded), so that a single time series of correlation coefficient is used to assess whether the NDVI and fAPAR have consistent timing anomalies (early versus late). This method enables to quantify the similarity of model and observed plant growth over the whole seasonal cycle, and in particular between the classical SOS, maximum of season and EOS. The correspondence of STI and total mass is investigated using the same method.

3. Results

3.1. Evaluation of modeled vegetation over the current period (2001-2014)

3.1.1. Mean annual cycle

The regional spatial structure of MODIS iNDVI, STI and vegetation masses simulated by STEP share similarities (*Figure 1*). The latitudinal gradient, primarily caused by the rainfall gradient, is observed in all maps (*Figure 1a* to *1d*), with larger values towards the south and the west. The northern edge of vegetation is located around 17°N in the west and 15°N in the east. The spatial correlation between iNDVI (resp. STI) and the total simulated mass at green vegetation maximum (resp. averaged over October-June) is r=0.69 (resp. r=0.57) for 2947 values. The simulations are less continuous than the satellite data, which is partly due to the model‘s sensitivity to soil texture (see *Figure 1e*) for plant germination, via the wilting point formulation.

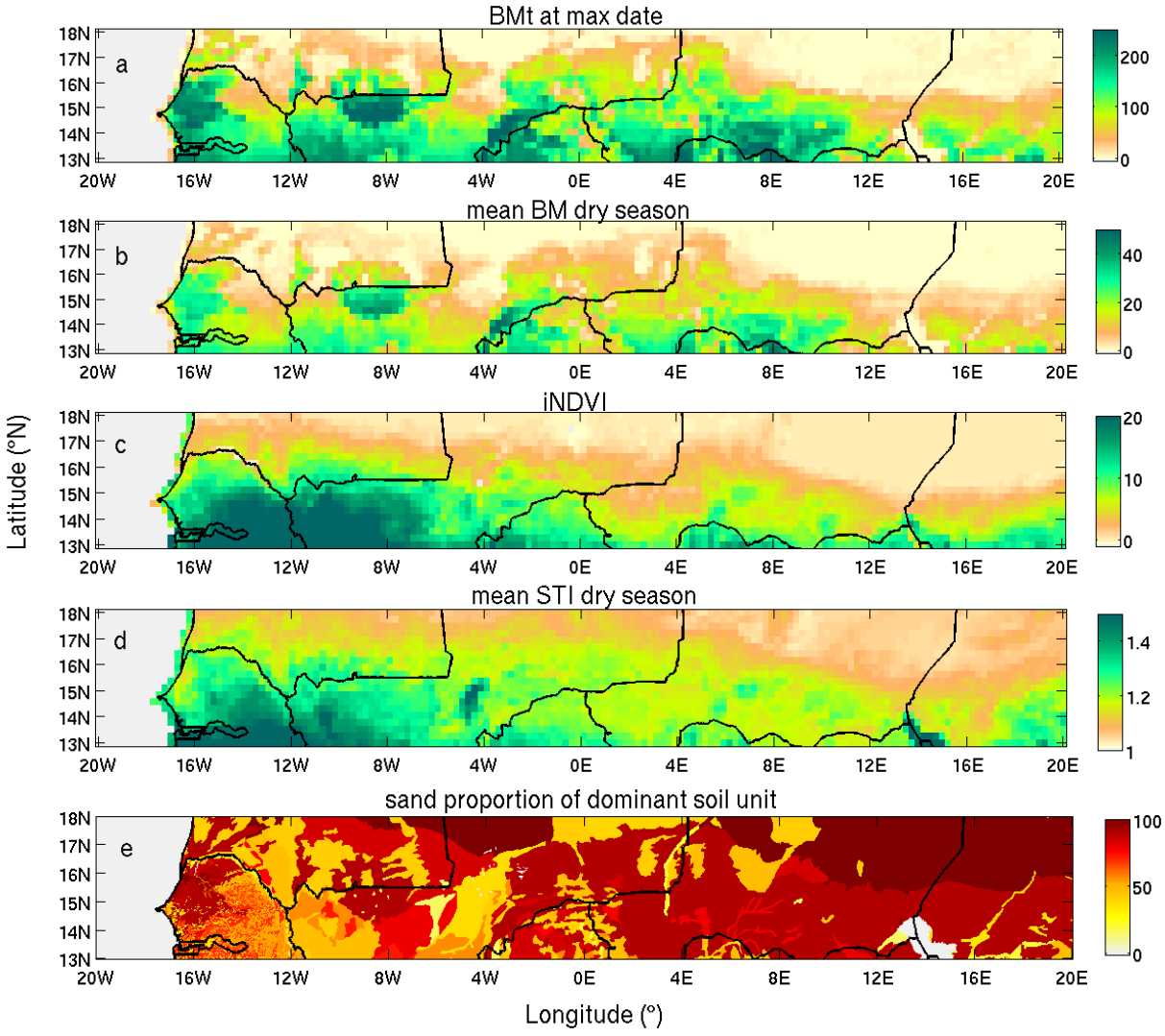

Figure 1: Mean values over 2001-2014 of:

(a) total simulated vegetation mass (g.m^{-2}) at green vegetation maximum; (b) total simulated vegetation mass (g.m^{-2}) averaged over October-June; (c) MODIS iNDVI; and (d) MODIS STI averaged over October-June; (e) is the topsoil sand proportion (%) of the dominant soil unit according to HWSD

The regional-mean vegetation cycle displays a marked seasonality, corresponding to the monsoonal rainfall dynamics, with vegetation starting to grow in June, peaking in early September and degrading from September to the next rainy season, as shown in both simulated vegetation mass and satellite indices (*Figure 2*). The mass of standing straws increases from July to early October, before gently decreasing when straws are being grazed or turned into litter. The correlation between simulated variables (continuous lines) and satellite-derived indices is significant for both green vegetation (r = 0.93 between fAPAR and NDVI, and r = 0.92 between model cover fraction and NDVI (not shown)) and total vegetation (r = 0.94 between total vegetation mass and STI, and r = 0.96 between green plus dry cover fraction and STI (not shown)). Simulated maxima occur a few days earlier than satellite-derived maxima: DoY 251 for green vegetation and DoY 254 for total vegetation compared to DoY 237 for NDVI and DoY 243 for STI.

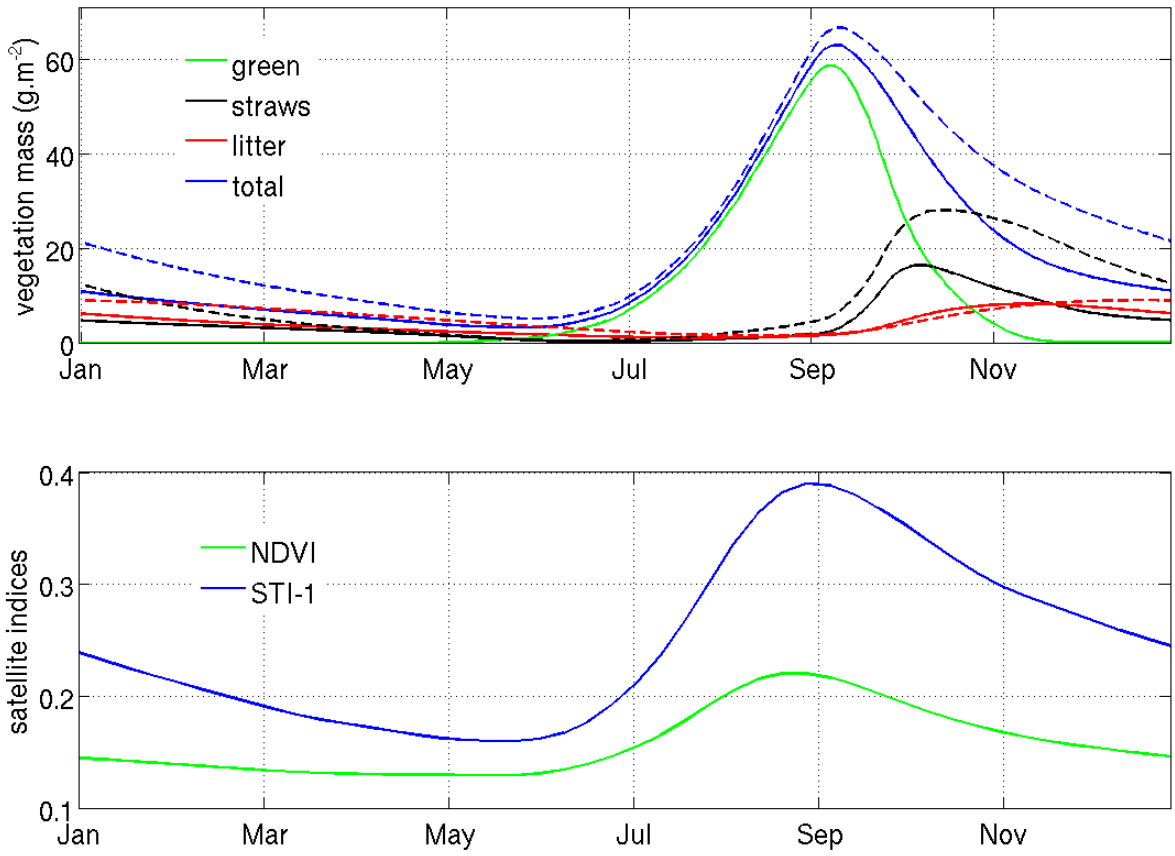

Figure 2: Regional-mean cycles of vegetation components simulated by STEP (top) and MODIS vegetation indices (bottom) for 2001-2014. Continuous (resp. dotted) lines

correspond to PV (resp. PV) simulations. For each date, the reported value is the mean of the 14 regional means over the study area.*

Simulation performed with PV climate forcing and grazing pressure of the 1960s shows that a lower grazing pressure (3 TLU.km^{-2} instead of 12 TLU.km^{-2}) has a significant impact on the dry vegetation. Straw mass peaks at almost 30 g.m^{-2} in October in PV*, compared to less than 20 g.m^{-2} in PV. The difference in litter mass is lower, averaging 5 g.m^{-2} over the whole dry season. The correlation of PV* total simulated vegetation mass with STI remains largely unchanged, since PV and PV* seasonal dynamics are rather similar.

3.1.2. Interannual variability

Simulated vegetation mass and MODIS indices exhibit a moderate interannual variability over the 2001-2013 period, with a standard deviation of about 20% of the 13-year average, except for STI during the dry season, which is remarkably stable. The simulated maximum total vegetation mass is about 90 g.m^{-2} (ranging between 60 and 120 g.m^{-2}) with a standard deviation of 16 g.m^{-2}, while the mean vegetation mass over the dry season is 10 g.m^{-2} (ranging between 5 and 14 g.m^{-2}) with a standard deviation of 2 g.m^{-2}. Similarly, the regional-mean iNDVI equals 5.8 (ranging between 4.3 and 7.4) with a standard deviation of 0.95, while the mean STI over the dry season is 1.2 (ranging between 1.2 and 1.25) with a standard deviation of 0.02. All these values exhibit similar values of the variation coefficient (about 0.18), except STI over the dry season (0.02).

The interannual variability of the regional mean is well captured by the model for both dry and rainy seasons (*Figure 3*). Significant correlations are obtained between iNDVI and total vegetation mass at green maximum ($r = 0.86$), and between STI and total vegetation mass over the dry season ($r = 0.84$). In addition, production anomalies between green and total vegetation are also well correlated, both between total vegetation at green maximum and STI over the dry season ($r = 0.83$), and between iNDVI and the simulated vegetation mass over the dry season ($r = 0.86$). However, some discrepancies are found: in 2008, the simulated vegetation mass increases compared to 2007, while satellite indices decrease. This is due to some scattered areas (located especially in southwestern Mali and Chad) over which STEP simulates higher mass in 2008, in response to higher rainfall. This anomaly dominates the regional-averaged signal, even if STEP simulations are lower elsewhere in 2008, namely from the north-west to the south-east of the area, in agreement with satellite estimates.

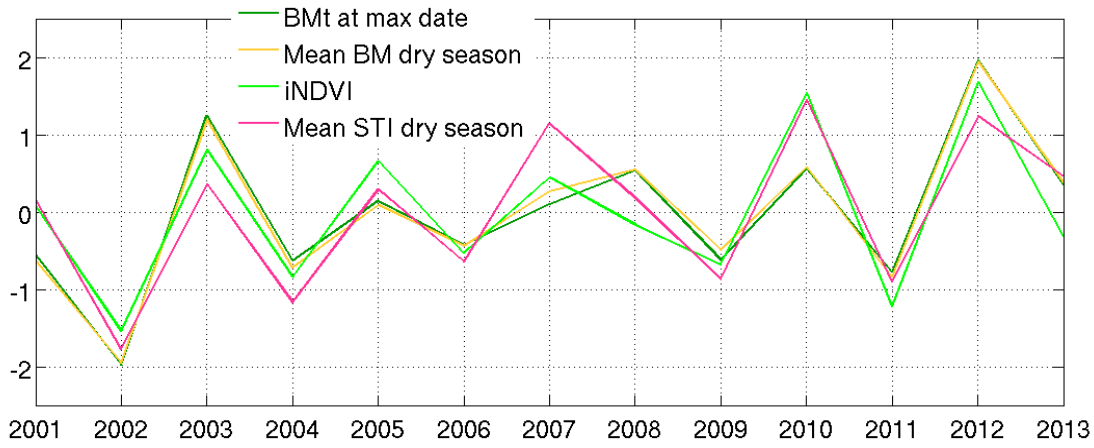

Figure 3: Deviations of the regional annual means from the 13-year regional average (2001-2013), normalized by the standard deviation for simulated vegetation masses and corresponding MODIS vegetation indices

To examine these results in more detail, time series of the anomalies are reported in *Figure 4*. Modeled anomalies correspond to STI anomalies (r = 0.66), but STI anomalies last longer. Extreme events, like the strong negative anomalies in 2002, 2004 and 2009, and strong positive anomalies in 2003, 2010 and 2012, are well captured by the model, particularly near the vegetation maximum. Most anomalies extend over the rainy season and the following dry season, but some short-lived anomalies reflect changes in phenology, such as an earlier growth in 2005, 2007 and 2008 and late growth in 2009.

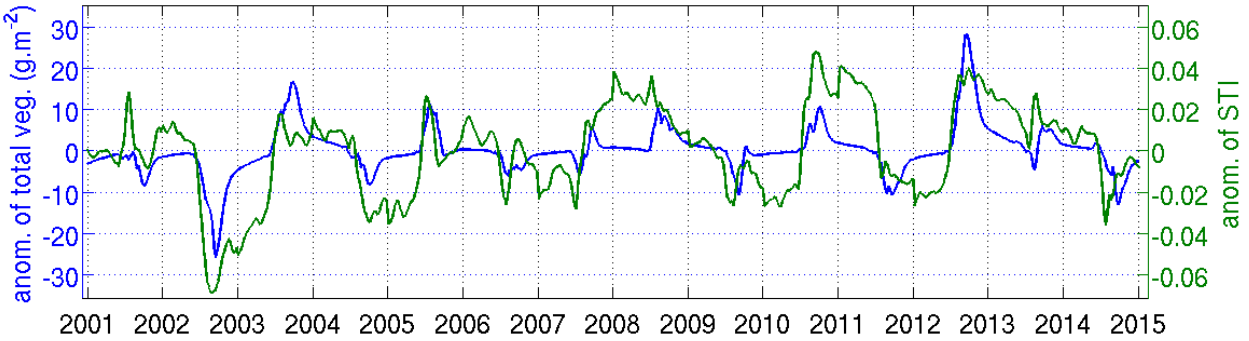

Figure 4: Anomalies of MODIS STI and total simulated vegetation mass from the regional-mean cycle over 2001-2014.

At a smaller spatial scale, the interannual variability of the vegetation is also well captured by the model (*Figure 5*). Correlation coefficients (r) are significant over 31% of the continental area between iNDVI and total vegetation at green maximum, and over 28% of the continental

area between STI and total vegetation mass averaged over the dry season. The correlations are homogeneously distributed, encompassing low and high vegetation masses, with similar spatial patterns for green and dry vegetation.

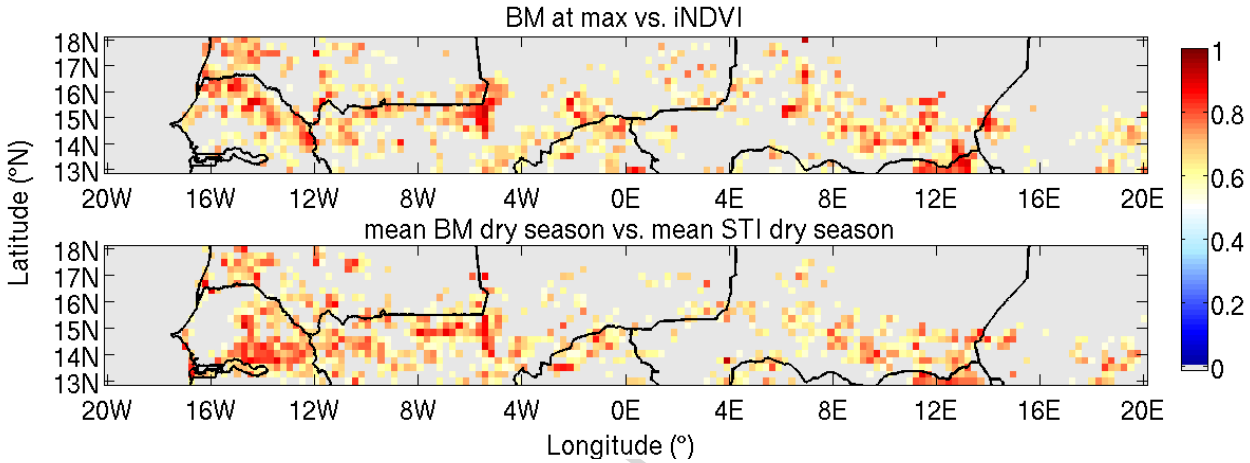

Figure 5: Correlation coefficient ($p<0.05$) over 2001-2014 between top: total simulated vegetation mass at green vegetation maximum and MODIS iNDVI bottom: total simulated vegetation mass and mean MODIS STI averaged over October to June

3.1.3. Phenology

According to the quantile-quantile analysis detailed in section 2.4, the interannual variability of growth and senescence stages is well represented by the model at the regional scale (*Table 2*). During the growth stage (DoY 170 to 220, i.e. July to mid-August), significant correlations are found between the time-variability of simulated fAPAR and observed NDVI, and between total vegetation mass and STI. The correlation is also good and significant during the senescence stage (DoY 280 to 310, i.e. early October to early November). During the end of the dry season, the correlation between total vegetation mass and STI is still relatively good, yet less significant. The correlation between the interannual variability in model outputs and satellite indices is noticeably high (r~0.90) at the beginning of vegetation growth (~DoY 200, mid-July) and at the end of vegetation senescence (~DoY 300, end of October), underlining the model's ability to simulate vegetation phenology accurately.

Table 2: Correlation between the time-variability of simulated fAPAR and MODIS NDVI, and total simulated vegetation mass and MODIS STI ($p<0.05$) (see section 2.4). x indicates non-significant values.

DoY	*170*	*180*	*190*	*200*	*210*	*220*	*280*	*290*	*300*	*310*
r(fAPAR, NDVI)	x	0.71	0.88	0.93	0.90	0.86	0.66	x	0.93	0.63
r(BMt, STI)	0.55	0.74	0.86	0.85	0.82	0.78	x	0.63	0.80	0.66

3.2. Phenological characteristics since 1960

Given that the main characteristics of the Sahelian annual vegetation growth and decay are well reproduced by the STEP model, the vegetation amounts and phenology are further examined using model outputs for the five historical periods defined in *Table 1*.

3.2.1. Mean values

The regional-mean vegetation cycles, averaged over each 6-year period (*Figure 6*, top), show contrasted amplitudes but relatively close dynamics. The amplitude of the mean P3 cycle is the weakest, barely reaching 30 $g.m^{-2}$, while the amplitude is largest in P1, which reaches around 78 $g.m^{-2}$. The other periods display intermediate amplitudes, with P5 (~55 $g.m^{-2}$) stronger than P2 (~40 $g.m^{-2}$) and P4 (~45 $g.m^{-2}$). Thus, the rainfall recovery during P4 and P5 has not been large enough to yield a mean vegetation cycle comparable to pre-drought conditions (P1). More precisely, the droughts shortened the vegetation cycle and reduced its amplitude before rainfall recovery (in P5) brought the start of the vegetation cycle back to a date similar to that of P1. However, the vegetation cycle in P5 still ends earlier than in P1. P2 and P4 exhibit close phasing, with senescence in P2 occurring faster than in P4. In P3, senescence occurs earlier than for all other periods. The number of vegetated grid cells (where vegetation mass exceeds 1 $g.m^{-2}$) is large in P1 (79% of the area), intermediate in P2 (74%), and then increases from a minimum in P3 (70%) to P4 (75%) and P5 (82%). The largest value in P5 is probably partly due to the rainfall data used in the simulation, since the krigged gauges measurements used in P1 to P4 are spatially smoother than the satellite-based data used in P5.

Differences among periods are mainly due to differences in mean rainfall during late June and from mid-July to early September, which are both higher in P1 than for all other periods (*Figure 6*, bottom). Mean rainfall amounts are comparable in P2, P4 and P5, yet with slightly larger values in P5 in June and from late August onwards. P3 rainfall has a lower maximum and decreases earlier (from the beginning of August) than in all other periods. Thus, after P1, the decrease in rainfall amounts during the early rainy season delayed the beginning of vegetation growth until P4. Rainfall amounts limited the length of the vegetation growing season in P3 in particular, but had less of an effect in P4, since the heavy rains at the core of the season lasted longer in P4 than in P3. The earlier start of vegetation cycle in P5 is likely due to the stronger rainfall in June.

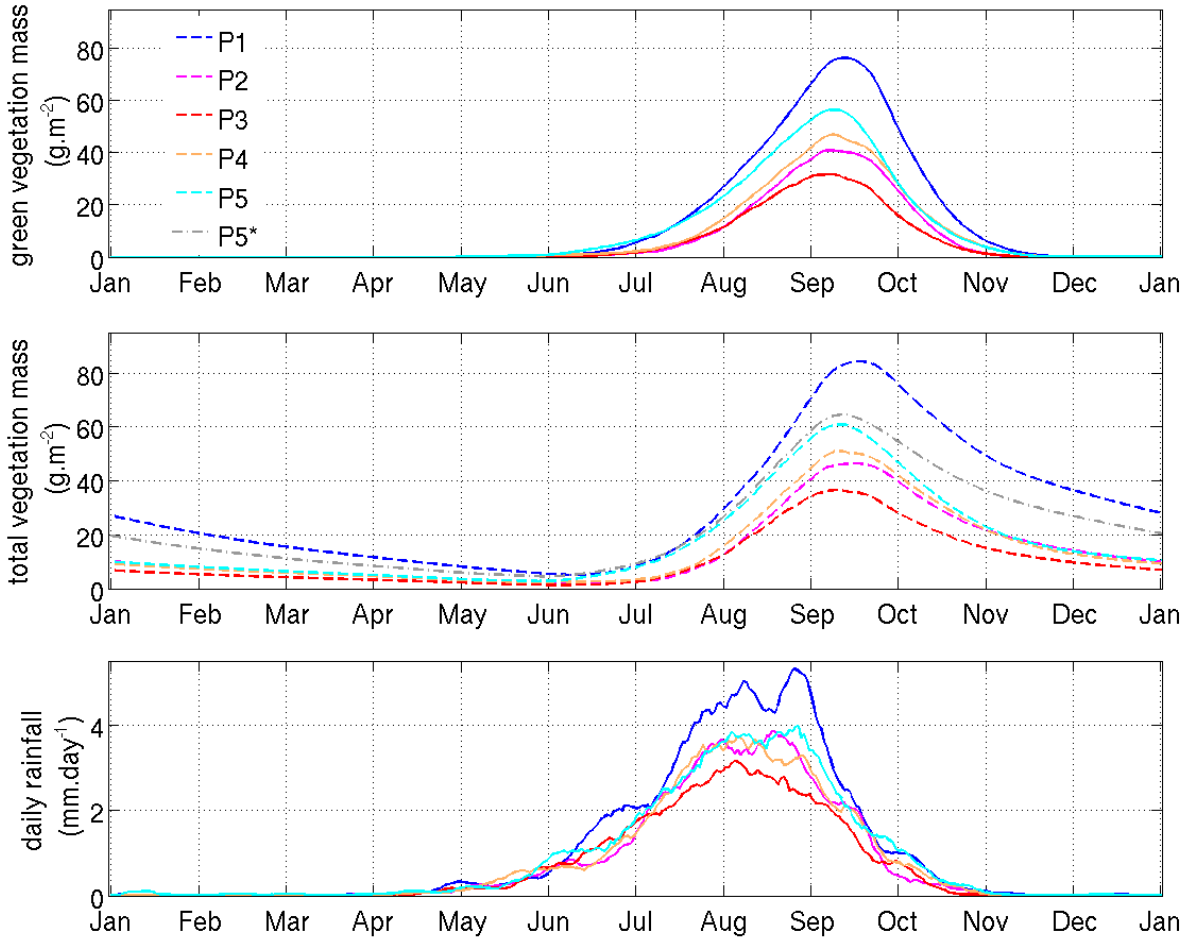

Figure 6: Regional- mean cycles of simulated vegetation mass (top: green vegetation; middle: total vegetation) and daily rainfall (11-days running mean) (bottom). For each DoY, the reported value is the mean of the 6 regional means over the study area. The annual regional-mean cumulated rainfall is much larger in P1 (391 mm) than in the other periods (288 mm (P2), 252 mm (P3), 294 mm (P4), and 328 mm (P5)).

The increase in grazing pressure results in a decreasing difference between total and green vegetation (*Figure 6*, middle). Green vegetation senescence (related to climate factors) is quicker in P2 than in P4 and P5 (*Figure 6*, top), but total vegetation decay is similar in P2, P4 and P5 from October onwards (*Figure 6*, middle), because of a lower grazing pressure in P2. Total vegetation masses in early September are of the same order in P5 and P5*, but they show an increasing difference during the beginning of the dry season (until December), with total vegetation mass in P5* noticeably larger than in P5, though lower than in P1.

Hovmoller diagrams of vegetation mass give further insight into the evolution of the annual cycle and its latitudinal dynamics for the different periods (*Figure 7*). The northern edge of the vegetated Sahel migrates southward from P1 (17°N) to P3 (16°N), and northward from P3

to P5 (16.5°N). In agreement with the seasonal cycle shown in *Figure 6* (middle), the P1 diagram displays a much longer vegetation cycle than all other periods: large masses are found until November up to 15°N, and during the dry season until about April. Differences in the seasonal cycle are particularly large between 14°N and 16°N with the earlier beginning (early July) and later ending (November) of the vegetation cycle in P1 and the earlier ending in P3 compared to all other periods. By contrast, the onset dates are similar in P2, P3 and P4. P5 growth begins earlier than in P4, particularly north of 14°N, but ends at the same time. The P5* vegetation cycle lasts longer than in P5, taking non-negligible values until March in the south of the area; yet it remains lower than in P1.

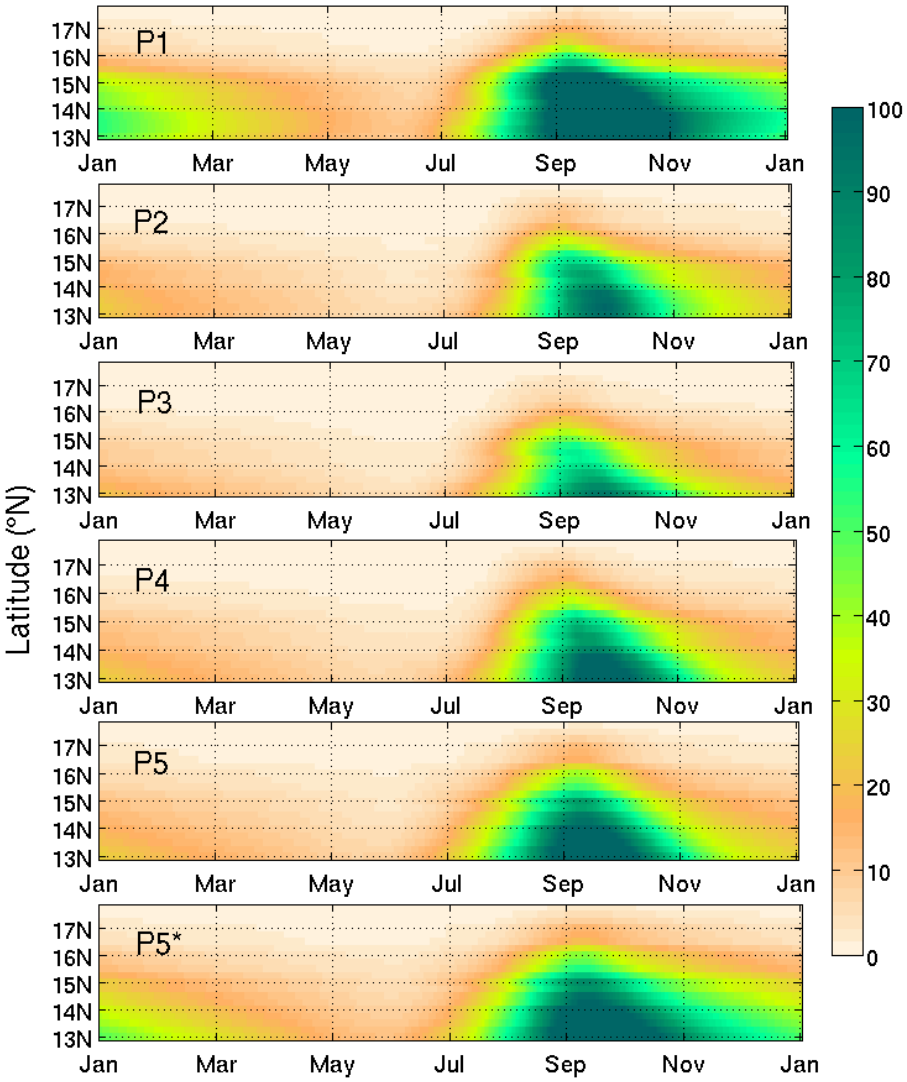

Figure 7: Hovmoller diagrams of simulated daily total vegetation mass ($g.m^{-2}$) averaged between 20°W and 20°E (mean over the 6 years for each period Pi).

The maps of the differences in vegetation mass between consecutive periods (*Figure 8*) illustrate how the changes in regional-mean cycles are spatially distributed within the Sahelian area. Vegetation mass decreases over the whole area between P1 and P2 by large amounts of about 40 to 100 g.m^{-2} (except in a small area located at 4.5°E, 17.5°N, where rainfall were nil during P1 but not P2). It further decreases between P2 and P3 – by lower amounts – over most of the area, except in the southwestern region and in some scattered locations in central Mali, northern Nigeria and Chad. The increase of vegetation mass from about 20 to 80 g.m^{-2} between P3 and P4, particularly important in southwestern Mali and South Mauritania, covers almost the whole study area, with the exception of northwestern and southern Senegal, extreme southwestern Mali and central Mali. Between P4 and P5, vegetation mass increases in some places (central south Niger, central and extreme southwestern Mali, and northwestern Senegal) but decreases in others (southwestern Mali, southwestern and eastern Niger, and Chad). This indicates that the regional vegetation recovery starting in P4 is occurring heterogeneously. The map of the difference of vegetation amounts between P1 and P5 (*Figure 8*, bottom) shows that current vegetation amounts are far below (by about 20 to 80 g.m^{-2}) pre-drought conditions over almost the whole area.

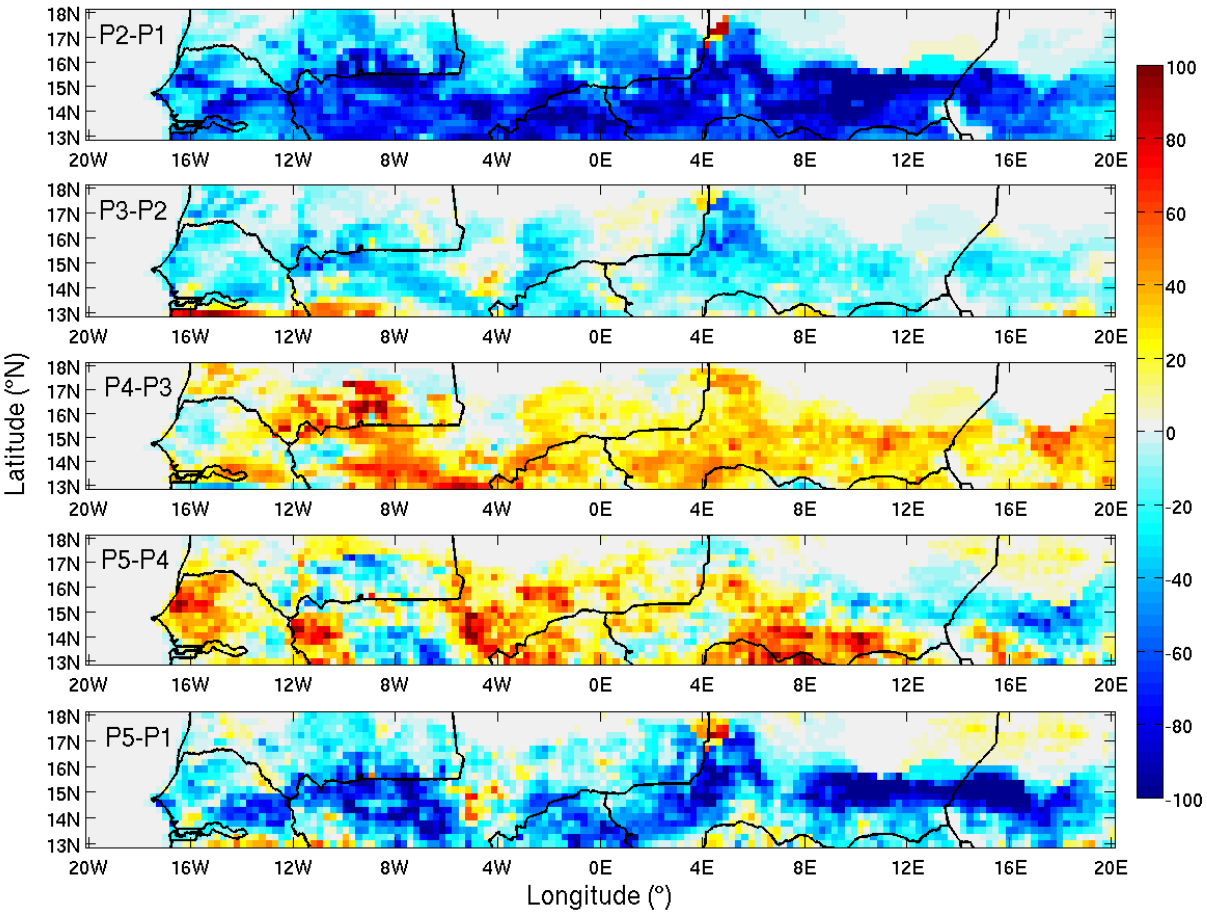

Figure 8: Differences (g.m^{-2}) between periods of the pluriannual mean of total simulated vegetation mass at green vegetation maximum

3.2.2. Inter-periods and interannual variability

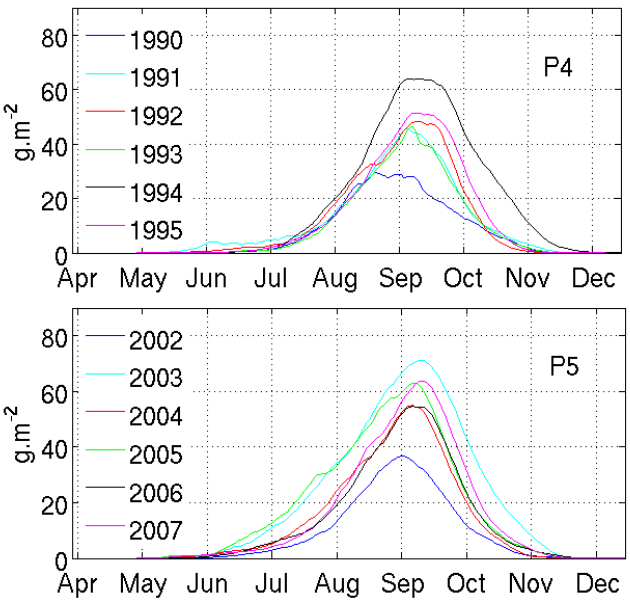

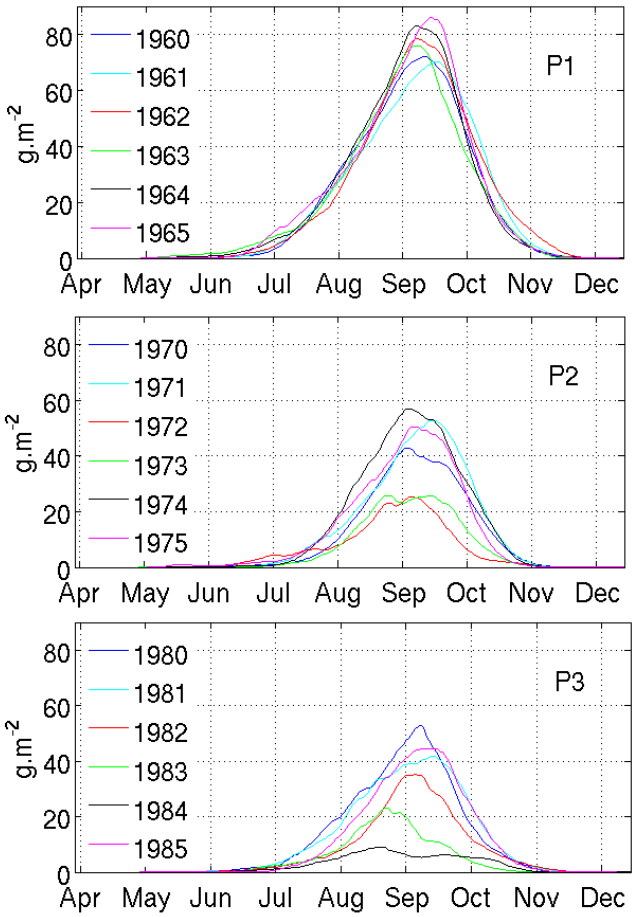

Figure 9: Regional-mean cycles. For each DoY, the reported value is the regional mean over the study area for each year of period Pi.

A strong interannual variability among the regional-mean annual vegetation cycles is noticeable within each period, except P1 (*Figure 9*). Droughts in 1972 and 1973 (P2) induce very low amplitudes of the vegetation cycles. In P3, this amplitudes decreases from 1980 to 1984, with 1984 by far the most dramatic year for all periods. Interannual variability is also important in P4 with a factor greater than 2 between the vegetation maximum mass in 1990 and 1994 (30 $g.m^{-2}$ against 64 $g.m^{-2}$). The interannual variability in P5 is somewhat lower than in P2, P3, and P4. Some years show the earlier beginning or the later ending of the green vegetation cycles observed in *Figure 6* (top) – such as 1994, which drives the later ending of P4 compared to P2 and P3; and 2003 and 2005, which account for the earlier beginning in P5 - tending slightly towards pre-drought conditions.

The normalized interannual variability of vegetation maximum mass is larger than that of annual rainfall amounts (*Table 3*). Indeed, the standard deviation of regional-mean annual rainfall ranges between 6% (P1) and 20% (P4) of the regional mean for the corresponding

periods, while the standard deviation of total vegetation mass at the date of green vegetation maximum ranges between 8% (P1) and 46% (P3) of the regional mean for the corresponding periods. More specifically, very dry years yield a regional mean of the vegetation maximum mass about 42% (1983) or 74% (1984) lower than the regional mean in P3, while, for the same years, regional-mean rainfall amounts are only about 21% lower than the regional mean in P3. Thus, at the interannual scale, vegetation does not linearly respond to rainfall, but decreases more sharply at the lowest rainfall rates encountered during the drought.

Table 3: Standard deviation (in %) of regional-mean annual rainfall and total simulated vegetation mass at the date of green vegetation maximum, normalized by the pluriannual regional mean for each period Pi

	P1	**P2**	**P3**	**P4**	**P5**
Rainfall	6	15	15	20	16
Total vegetation	8	33	46	23	20

3.2.3. Phenology

Spatial distribution of phenological dates is presented in Period P2 as an example (*Figure 10*). SOS exhibit patterns related to the rainfall gradient and to large soil structures. Indeed, the main south-north gradient with later SOS in the north (DoY 220, early August) than in the south (DoY 130, early May) broadly echoes the latitudinal structure of rainfall onset dates over the Sahel (e.g. *Fitzpatrick et al.*, 2015). The SOS also appears sensitive to the soil type. In particular, regions corresponding to early SOS in the south of the study area correspond to very sandy soils (see *Figure 1e*), while SOS occurs later over small spots of loamy and clayed soils. The rainfall gradient is also clearly reflected into the dates of green vegetation maximum, EOS and LOS. Maximum dates and EOS exhibit smooth spatial gradients, from the maximum occurring at DoY 220 (early August) and EOS a few days later in northeastern Sahel, to the maximum occurring at DoY 270 (late September) and EOS at DoY 320 (mid-November) in southwestern Sahel. Consequently, LOS ranges between a few days in the north to about 150 days in the south.

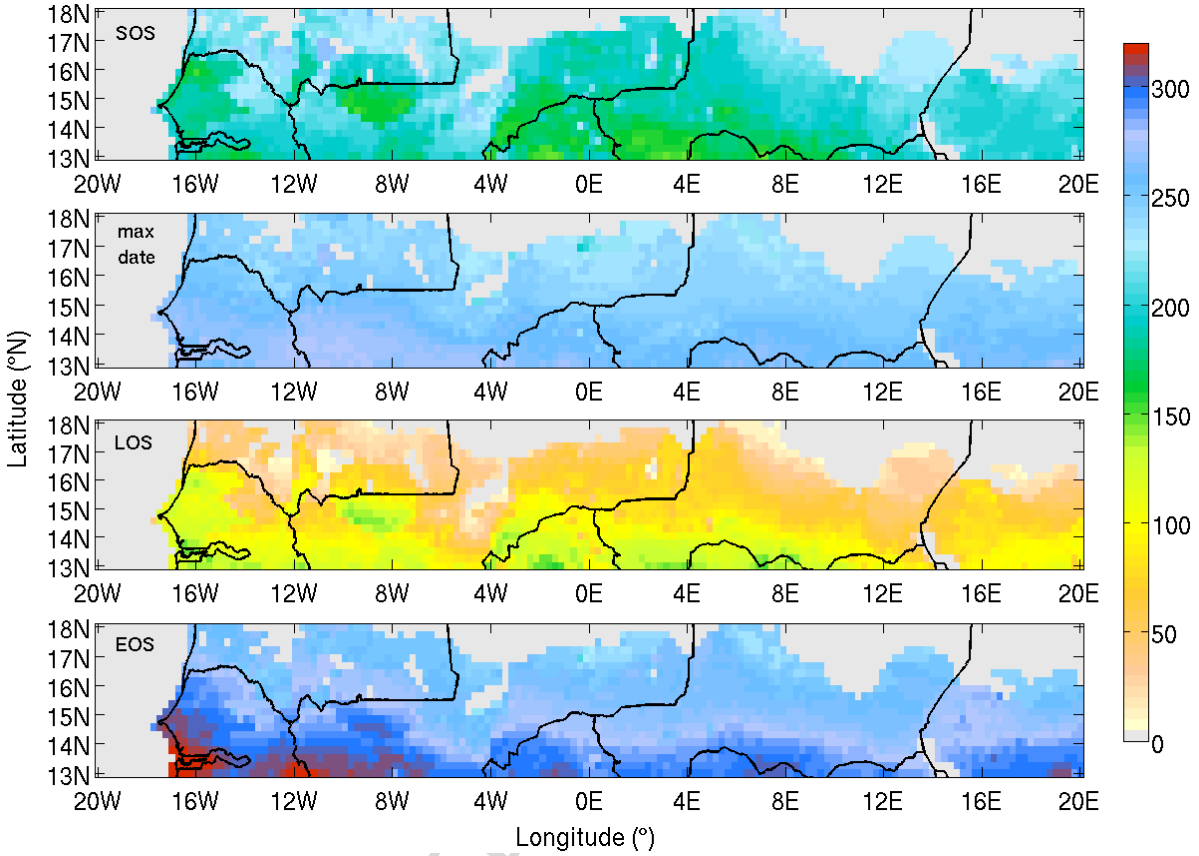

Figure 10: Dates of Start of Season (SOS, in DoY), green vegetation maximum (in DoY), Length of Season (LOS, in days) and End of Season (EOS, in DoY), averaged over period P2

Regional-mean phenological characteristics are reported in *Table 4*. The values are computed over grid cells where simulated vegetation mass exceeds 1 $g.m^{-2}$ for all years of all periods (n = 11 291, corresponding to 64% of the continental area). SOS substantially increases from P1 to P2 and decreases from P4 to P5 (by about 10 days), whereas it remains relatively stable from P2 to P4. The season in P1 (resp. P3) ends about 10 days later (resp. earlier) than in P2, P4 and P5. The date of minimum vegetation mass, which typically occurs around the end of the dry season, is not independent of the timing of the following vegetation cycle, i.e. of the date of vegetation growth beginning. Indeed, it generally occurs a few days before the SOS. Maximum and EOS both occur earlier from P1 to P3 and later from P3 to P5. Consequently, LOS is strongly decreasing from P1 to P2 (24 days) and from P2 to P3 (9 days), before increasing from P3 to P4 and from P4 to P5 by 13 and 12 days, respectively. The standard deviation of these regional-mean dates is the largest for EOS (and LOS) and the lowest for maximum and minimum dates.

Table 4: Regional-mean phenological characteristics over the periods Pi

	P1	**P2**	**P3**	**P4**	**P5**	std
Green vegetation SOS (DoY)	181	192	191	189	180	6.0
Green vegetation maximum date (DoY)	259	253	245 253		251	4.9
Green vegetation EOS (DoY)	291	279	269	280	283	8.1
Green vegetation LOS (days)	111	87	78	91	103	13.1
Total vegetation minimum date (DoY)	179	187	182	185	177	4.2

In terms of spatial distribution, phenological dates show contrasted dynamics in the western, central and eastern Sahel, delimited approximately by 4°W and 12°E, with specific changes near the coast (Senegal) and at the eastern edge of the West African monsoon area (Chad). Thus, the trends reported in *Table 4* are not spatially homogeneous and involve differences in sub-regional dynamics (not shown). For example, the later SOS in P2 compared to P1 is widely spread over the Sahel (but more pronounced eastward), while the earlier SOS in P5 compared to P4 is mostly driven by the southeastern Sahel SOS (16°E to 20°E, between 13°N and 15°N). Similarly, the slightly earlier SOS in P3 (resp. P4) compared to in P2 (resp. P3) is driven by the earlier SOS over an area east of 12°E (resp. east of 4°W). Altogether, changes in SOS west of 4°W are very low through all periods, with the exception of a short advance in P5.

Similarly, the earlier maximum in P1 compared to P2 (resp. P2 compared to P3) is mainly concentrated within a wide central area north of 14°N (resp. in the area east of 4°W). The advance of EOS from P1 to P3 is more pronounced southward. As a consequence, the decrease of LOS mostly occurs south of 15°N and east of 12°E from P1 to P2, and west of 4°W from P2 to P3. Then LOS increases over the whole study area between 13°N and 15°N from P3 to P4 and west of 12°W and in south-central Sahel from P4 to P5.

The spatial distribution of the variability of phenological dates gives further information on the vegetation dynamics, complementary to regional means in *Table 4*. SOS is the most variable date for all periods over a large part of the study area (38 to 57% of this area, in P3 and P5 resp.), particularly in the central part (*Figure 11*). Its standard deviation is the largest in P5 (the regional mean of this variability is 22 days) and the lowest in P1 (15 days). SOS variability is strongest in P3 and P5. This spatial variability is consistent with the high heterogeneity of the rainfall monsoon onset over the Sahel (*Fitzpatrick et al.,* 2015). These

results contrast with the regional means of phenological dates, with SOS among the least variable dates (*Table 4*), and suggests that SOS varies strongly locally, while its regional mean value remains relatively stable among periods.

The date of green vegetation maximum is the most variable date in some scattered places over the entire area (4 to 10% of the study area, in P4 and P1 resp.), including at the northern edge of the vegetated area (in P1, P2, P5), in Senegal (in all periods) and in some places at the very south of the study area (in P3). Its average standard deviation is largest in P3 (16 days) and lowest in P1 (10 days). EOS is the most variable date in some specific areas (14 to 22% of the study area, in P1 and P4 resp.), mostly in an area located southeast in P2 and P3 (16°E to 20°E), shifting west in P4 (12°E to 16°E) and disappearing in P5. This corresponds to sandy areas where SOS varies little during P3 and P4, while EOS varies a lot (particularly in 1984 as compared to the other years in P3, and between 1990 and 1994 in P4). Another such region is located southeast of Gambia, especially in P1, P2 and P4. The mean variability of EOS is the largest in P3 (17 days) and the lowest in P1 (10 days). Additionally, the variability of SOS, maximum date and EOS is lowest in P1 (not shown); for all periods, the maximum date is the least variable date.

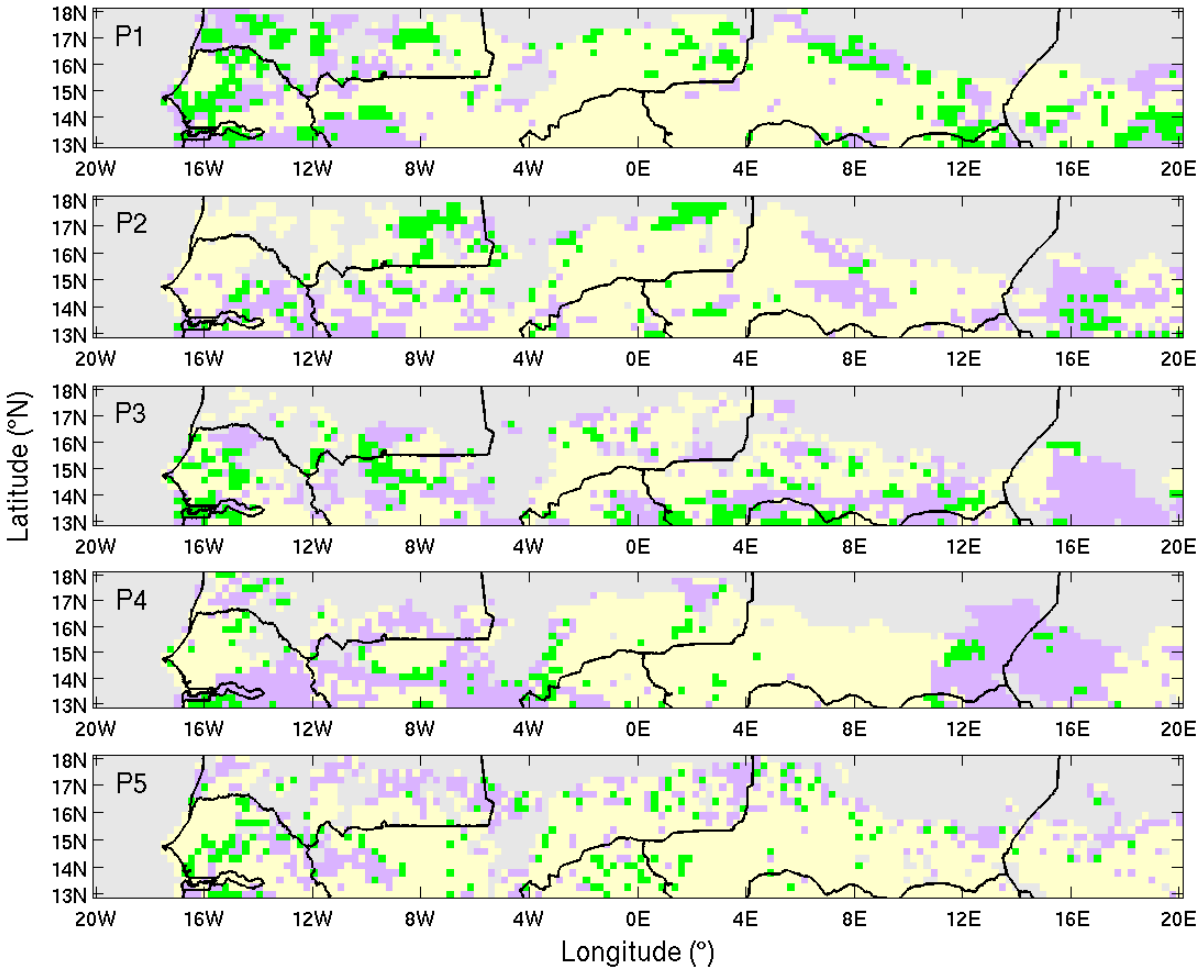

Figure 11: Most interannually variable date (ranged according to their standard deviation, in days) within each period Pi (yellow: SOS; green: maximum date; pink: EOS)

Phenological dates (SOS, EOS and LOS) display a similar dependency to annual rainfall amounts among periods (not shown). The larger the rainfall amount, the earlier the vegetation SOS, and the later the EOS. The relation between phenology and rainfall is less linear in P5 for SOS, in P3 for EOS and LOS, and in P1 for vegetation mass maximum. EOS, LOS and vegetation mass maximum all tend towards asymptotic values when rainfall exceeds about 700 $mm.yr^{-1}$: vegetation mass rarely exceeds 250 $g.m^{-2}$ even for larger rainfall.

Table 5: Correlation coefficient (r) between annual rainfall amounts and characteristic values of the vegetation cycle over the periods Pi

	P1	**P2**	**P3**	**P4**	**P5**
Total vegetation mass at green vegetation maximum	*0.49*	*0.53*	*0.65*	*0.65*	*0.69*
SOS	-0.26	-0.28	-0.23	-0.25	-0.30
LOS	0.61	0.60	0.58	0.58	0.58
EOS	0.70	0.69	0.69	0.69	0.63

Correlations for the same grid cells as in *Table 4* are reported in *Table 5*. SOS is weakly anticorrelated to annual rainfall, probably because of the importance of soil texture for seasonal grass germination, as underlined by *Bobée et al.* (2012). Thus, SOS depends on both rainfall and soil texture. Both total vegetation mass and EOS are well correlated with rainfall amounts. A slight and constant increase (resp. decrease) in the correlation between rainfall and total vegetation mass at green maximum (resp. EOS) is observed from P1 to P5, probably because of the more limiting effect of rainfall amount during droughts, as well as its increasing variability.

4. Discussion and Conclusion

The objective of this study was to analyze how the Sahelian rainfall variability since 1960, including the droughts of the 1970s and 1980s, affected the phenology of the annual herbaceous vegetation, during both wet and dry seasons. This cannot be achieved solely from satellite data, which is only available starting from the 1980s. Therefore, in order to explore this longer time range, the annual vegetation was simulated by the STEP model, which was specifically designed to represent the Sahelian annual grass cycle.

STEP results were evaluated through comparison with MODIS vegetation indices over the 2001-2014 period. This demonstrated the model's ability to reproduce the observed regional-mean annual vegetation cycles and their interannual variability for both green and dry vegetation. Additionally, the model accurately captures the main positive and negative anomalies over 2001-2014, though the simulated anomalies do not last as long as in satellite observations. Further, the model is able to simulate the observed regional and interannual variability of vegetation growth and senescence stages, making it suitable for describing long-term vegetation changes in the semi-arid Sahel, particularly in terms of annual grass phenology.

The inclusion of the vegetation dynamics during the dry season represents a major step forward, and the first comparisons with dry-season satellite-based indices are very promising for further validation at a regional scale. The simulations display a higher sensitivity to soil texture than observed via satellite. The use of local observations of soil texture as input could help clarify whether this is due to uncertainty in the HWSD soil database or to the model's over-sensitivity to this parameter.

The analysis of vegetation changes since 1960 shows that, despite the partial rainfall recovery and the observed re-greening since the 1990s, the present vegetation cover is still far below its pre-drought levels. This is in broad agreement with the changes in rainfall amounts over the same period (*Lebel and Ali*, 2009). The simulated regional-mean vegetation cycles are also in agreement with the observations reported by *Anyamba and Tucker* (2005), who analyzed Advanced Very High Resolution Radiometer (AVHRR) NDVI over 1982-2003, and distinguished the 1982-1993 period, with vegetation below average, from the 1994-2003 period, with higher values of vegetation. In addition, the wet year 1994 and the dry year 2002, identified by *L'Hôte et al.* (2002) from rainfall measurements, exhibit respectively large and low vegetation mass in the STEP simulations.

The present study gives further information on the vegetation cover since 1960. The droughts of the 1970s and 1980s shortened the annual vegetation cycle and reduced its amplitude, while the subsequent rainfall recovery yielded a start of the vegetation cycle at a date similar to that of the 1960s. However, the current vegetation cycle still ends earlier than in the 1960s. The vegetation decrease after the droughts in the 1970s was large and extended over the whole Sahelian area, and was even more pronounced during the 1980s in Central Sahel. Since then, the vegetation recovery has been spatially heterogeneous. From 1980s to 1990s, the Sahelian "re-greening" was mainly located in the southern half of Niger, southwestern Mali, and south-central Chad. Between the 1990s and 2000s, trends in vegetation mass were

positive in south-central Niger, northwestern Senegal, and central Mali (consistently with *Dardel et al.,* 2014a), and negative in southwestern Mali, southwestern and eastern Niger, and Chad.

Moreover, current dry vegetation mass has been shown to be lower than in the pre-drought period. This is partly due to the increasing grazing pressure since 1960. Indeed, dry vegetation exhibits a faster decrease for recent and current periods because of this increasing grazing pressure. As a consequence, while the green vegetation mass peaks at higher values in the 2000s than in the 1970s and 1980s, the regional-mean vegetation mass during the dry season has roughly the same values for all these periods. Thus, despite the relative rain and vegetation recovery, forage availability for livestock has not necessarily been increasing since 1990. This might have strong impacts on herders' strategies, especially at the end of the dry season when resources are the scarcest.

Knowledge of dry season vegetation is also critical in estimating the surface sensitivity to wind erosion (e.g. *Pierre et al.,* 2015). Indeed, the green vegetation cover due to the Sahelian re-greening since the 1990s probably partly inhibited wind erosion during the early rainy season, while the concomitantly increasing grazing pressure deprived the surface of protection by vegetation at the end of the dry season. Altogether, the current Sahelian surface is very likely more prone to wind erosion now than before the 1970s and 1980s droughts. This phenomenon might have in turn impacted the soil nutrient content, and therefore feedback on vegetation productivity, by removing or depositing fine particles of the soil (e.g. *Sterk et al.,* 1996; *Bielders et al.,* 2002; *Herrmann et al.,* 2010).

Concerning phenology, the increasing simulated vegetation maximum from 1980s to 2000s is in agreement with results from *Heumann et al.* (2007), which indicate that the Sahelian "re-greening" is due to an increase in the amplitude of the seasonal growth cycle. Yet, the present results also indicate a lengthening of the Sahelian growing season since the 1980s, which was noted by these authors in the Sudan and Guinean regions only. This suggests that changes in SOS and EOS also had an impact on Sahelian vegetation trends, although a clear time shift in the vegetation cycle is not observed. This does not preclude the possibility of a future time shift, as would be expected from the delayed Sahelian monsoon rainfall identified by *Biasutti and Sobel* (2009) in climate projections. However, our results indicate that such a lag in the vegetation cycle did not develop during the past 50 years.

Since the 1970s, Sahelian vegetation has also been characterized by increased interannual variability, which is relatively higher for maximum vegetation mass than for annual rainfall, possibly because of the impact of rainfall distribution throughout the rainy season on

vegetation growth. EOS, LOS and maximum vegetation mass also exhibit an upper limit when rainfall exceeds approximately 700 $mm.yr^{-1}$. This limit is of the same order as the upper limit of 800 $mm.yr^{-1}$ observed by *Prince et al.* (2007), beyond which the RUE (Rainfall Use Efficiency, i.e. the vegetation productivity per rainfall amount) starts decreasing.

The variability of regional-mean phenological dates (SOS, maximum date and EOS) is lowest in the 1960s. For all periods, the maximum date is the least variable date over most of the area as well as among regional-mean phenological dates, which is consistent with findings by *Heumann et al.* (2007) for the more recent 1982-2005 period. Further, the high interannual variability of LOS, increasing northwards, is in agreement with *Meroni et al.* (2014). The regional-mean SOS is the least variable date among all periods, but at the more local scale, SOS is the date with the most fluctuation. The large variability of SOS (with a typical range of 26 days) is in agreement with findings by *Bégué et al.* (2014), who obtained an SOS variability of 22 to 30 days in southern Mali, based on MODIS observations. SOS appears to be strongly dependent on the soil texture, probably because a given amount of soil water is required for germination in the model, leading to a threshold effect which is likely less abrupt in reality.

Results from this work could be refined by improving forcing datasets and model parameterizations. Firstly, concerning forcing datasets, *Pierre et al.* (2011) showed that the simulated vegetation was the more sensitive to rainfall and soil texture, while this study underlines the sensitivity to grazing pressure. For the latter forcing, it would be useful to take into account the spatial, seasonal and interannual variability of the grazing pressure, particularly during droughts. Indeed, the values used here are a first estimation of the Sahelian grazing pressure, and further efforts would be required to obtain more reliable values directly from national and subnational censuses.

Secondly, in terms of parameterization, it is likely that a more complete picture of Sahelian vegetation changes would be obtained through the introduction of the woody population in the model. Indeed, even though the variability of annual grass phenology dominates (*Archibald and Scholes*, 2007), the Sahelian tree cover might have changed since 1960 (e.g. *Wardell et al.*, 2003; *Hiernaux et al.*, 2009b).

Croplands represent only a small percentage of the Sahelian area (e.g. *Ramankutty*, 2004). However, taking into account land use would also improve the present work, since crops and natural grass might have slightly different phenologies. Finally, it would be interesting to quantify the changes in nutrient availability, vegetation composition, and runoff in the Sahel,

so as to better represent past changes in vegetation productivity in the Sahel, and thus to provide further insight into land degradation and vegetation resilience in semi-arid areas.

Acknowledgments

This work was supported by the research program CAVIARS (ANR-12-SENV-0007-01) of the French Agence Nationale de la Recherche. Rainfall gauge measurements were provided by the AGHRYMET Regional Centre (Centre Régional de Formation et d'Application en Agrométéorologie et Hydrologie Opérationnelle, Niamey, Niger) and processed by the LTHE (Laboratoire d'étude des Transferts et d'Hydrologie en Environnement, Grenoble, France). We thank G. Quantin for providing helpful information about this rainfall dataset, as well as C. Delon and M. Diawara for providing parameterizations that represent the dry vegetation, and all colleagues involved in the CAVIARS project for their useful comments on the present work.

References

Anyamba, A., and C. J. Tucker, 2005: Analysis of Sahelian vegetation dynamics using NOAA-AVHRR NDVI data from 1981-2003, *J. Arid Environ*., 63, 596-614.

Archibald, S., and R. J. Scholes, 2007: Leaf green-up in a semi-arid African savanna – separating tree and grass responses to environmental cues, *J. Veg. Sci*., 18, 583-594.

Begue, A., E. Vintrou, A. Saad, and P. Hiernaux, 2014: Differences between cropland and rangeland MODIS phenology (start-of-season) in Mali, *Int. J. Appl. Earth Obs. Geoinf*., 31, 167-170.

Berg, A., B. Sultan, and N. de Noblet-Ducoudre, 2011: Including tropical croplands in a terrestrial biosphere model: application to West Africa, *Clim. Chang*., 107, 755-782.

Biasutti, M., and A. H. Sobel, 2009: Delayed Sahel rainfall and global seasonal cycle in a warmer climate, *Geophys. Res. Lett*., 36, L23707, doi: 10.1029/2009GL041303.

Bielders, C. L., J.-L. Rajot, and M. Amadou, 2002: Transport of soil and nutrients by wind in bush fallow land and traditionally managed cultivated fields in the Sahel, *Geoderma* 109, 19–39.

Bobée, C., C. Ottlé, F. Maignan, N. de Noblet-Ducoudré, P. Maugis, A.-M. Lézine, and M. Ndiaye, 2012: Analysis of vegetation seasonality in Sahelian environments using MODIS LAI, in association with land cover and rainfall, *J. Arid Environ.*, 84, 38-50.

Bondeau, A., D. W. Kicklighter, J. Kaduk, and the participants of the Potsdam NPP model intercomparison, 1999: Comparing global models of terrestrial net primary productivity (NPP): importance of vegetation structure on seasonal NPP estimates, *Glob. Change Biol.*, *5*(S1), 35-45.

Brender, P., P. Ciais, C. Ottle, P. Hiernaux, E. Mougin, L. Kergoat, F. Chevallier, and P. Peylin, 2011: Evaluation and improvement of the representation of Sahelian savannah in the vegetation model ORCHIDEE, *in* Africa and the carbon cycle, *World Soil Resources Support*, Bombelli A. and Valentini R. Eds, Rome, 105, 95-101.

Butt, B., M. D. Turner, A. Singh, and L. Brottern, 2011: Use of MODIS NDVI to evaluate changing latitudinal gradients of rangeland phenology in Sudano-Sahelian West Africa, *Remote Sens. Environ*., 115, 3367-3376.

Cayrol, P., L. Kergoat, S. Moulin, G. Dedieu, and A. Chehbouni, 2000: Calibrating a coupled SVAT-vegetation growth model with remotely sensed reflectance and surface temperature-A case study for the HAPEX-Sahel grassland sites, *Journ. Appl. Meteorol.*, *39*(12), 2452-2472.

Choler, P., W. Sea, and R. Leuning, 2011: A benchmark test for ecohydrological models of interannual variability of NDVI in semi-arid tropical grasslands, *Ecosystems*, 14, 183-197.

Ciret, C., J. Polcher, and X. Le Roux, 1999: An approach for simulating the phenology of savanna ecosystems in the Laboratoire de Meteorologie Dynamique general circulation model, *Glob. Biogeochem. Cycles*, 13(2), 603-621.

Dardel, C., L. Kergoat, P. Hiernaux, E. Mougin, M. Grippa, and C. J. Tucker, 2014a: Re-greening Sahel: 30 years of remote sensing data and field observations (Mali, Niger), *Remote Sens. Environ.*, 140, 350-364.

Dardel, C., L. Kergoat, P. Hiernaux, M. Grippa, E. Mougin, P. Ciais, and C. C. Nguyen, 2014b : Rain-use-efficiency: What it tells us about the conflicting Sahel greening and Sahelian paradox, *Remote Sens.*, *6*(4), 3446-3474.

Daughtry, C., and M. Quemada, 2015: Assessing crop residue cover when scene moisture conditions change, *Geoscience and Remote Sensing Symposium* (*IGARSS*), 4652-4655, IEEE.

Delon, C., E. Mougin, D. Serça, M. Grippa, P. Hiernaux, M. Diawara, C. Galy-Lacaux, and L. Kergoat, 2015: Modeling the effect of soil moisture and organic matter degradation on biogenic NO emissions from soils in Sahel rangeland (Mali), *Biogeosciences*, 12, 3253-3272, doi:10.5194/bg-12-3253-2015.

Dicko, M. S., M. A. Djiteye, and M. Sangare, 2006: Les systèmes de production animale au Sahel, *Secheresse*, 17, 83-97.

Diouf, A., and E. F. Lambin, 2001: Monitoring land-cover changes in semi-arid regions: remote sensing data and field observations in the Ferlo, Senegal, *J. Arid Environ.*, *48*(2), 129-148.

Fensholt, R., I. Sandholt, and M. Schultz Rasmussen, 2004: Evaluation of MODIS LAI, fAPAR and the relation between fAPAR and NDVI in a semi-arid environment using in situ measurements, *Remote Sens. Environ.*, 91(3), 490-507.

Fensholt, R., K. Rasmussen, T. T. Nielsen, and C. Mbow, 2009: Evaluation of earth observation based long term vegetation trends - Intercomparing NDVI time series trend analysis consistency of Sahel from AVHRR GIMMS, Terra MODIS and SPOT VGT data, *Remote Sens. Environ.*, *113*(9), 1886-1898.

Fischer, G., F. Nachtergaele, S. Prieler, H.T. van Velthuizen, L. Verelst, and D. Wiberg, 2008: *Global Agro-ecological Zones Assessment for Agriculture (GAEZ 2008),* IIASA, Laxenburg, Austria and FAO, Rome, Italy.

Fitzpatrick, R. G. J., C. L. Bain, P. Knippertz, J. H. Marsham, and D. J. Parker, 2015: The West African monsoon onset: A concise comparison of definitions, *J. Climate*, *28*, 8673–8694, doi: 10.1175/JCLI-D-15-0265.1

Frison, P. L., E. Mougin, and P. Hiernaux, 1998: Observations and interpretation of seasonal ERS-1 wind scatterometer data over Northern Sahel (Mali), *Remote Sens. Environ*., 693, 233-242.

Gibelin, A.-L., J.-C. Calvet, J.-L. Roujean, L. Jarlan, and S. O. Los, 2006: Ability of the land surface model ISBA-A-gs to simulate leaf area index at the global scale: Comparison with satellite products, *J. Geophys. Res.,* 111, D18102, doi: 10.1029/2005JD006691.

Guerschman, J.P., M.J. Hill, L.J., Renzullo, D.J., Barrett, A.S.., Marks, and E.J., Botha, 2009: Estimating fractional cover of photosynthetic vegetation: non-photosynthetic vegetation and bare soil in the Australian tropical savanna region upscaling the EO-1 Hyperion and MODIS sensors, *Remote Sens. Environ*., 113, 928–945.

Hein, L., and N. de Ridder, 2006: Desertification in the Sahel: a reinterpretation, *Glob. Change Biol.*, 12(5), 751-758.

Herrmann, S. M., A. Anyamba, and C. J. Tucker, 2005: Recent trends in vegetation dynamics in the African Sahel and their relationship to climate, *Glob. Environ. Chang*., 15, 394-404.

Herrmann, L., R. Jahn, and T. Maurer, 2010: Mineral dust around the Sahara – from source to sink. A review with emphasis on contributions of the German soil science community in the last twenty years, *J. Plant Nutr. Soil Sci*., 173, 811-821.

Heumann, B. W., J. W. Seaquist, L. Eklundh, and P. Jönsson, 2007: AVHRR derived phenological change in the Sahel and Soudan, Africa, 1982-2005, *Remote Sens. Environ*., 108, 385-392.

Hickler, T., L. Eklundh, J. W. Seaquist, B. Smith, J. Ardö, L. Olsson, M. T. Sykes, and M. Sjöström, 2005: Precipitation controls Sahel greening trend, *Geophys. Res. Lett*., 32, L21415, doi: 10.1029/2005GL024370.

Hiernaux, P., A. Ayantunde, A. Kalilou, E. Mougin, B. Gérard, F. Baup, M. Grippa, and B. Djaby, 2009a: Resilience and productivity trends of crops, fallows and rangelands in Southwest Niger: impact of land use, management and climate changes, *J. Hydrol*., AMMA CATCH special issue, 375(1-2), 65-77.

Hiernaux, P., L. Diarra, V. Trichon, E. Mougin, N. Soumaguel, and F. Baup, 2009b: Woody plant population dynamics in response to climate changes from 1984 to 2006 in Sahel (Gourma, Mali), *J. Hydrol.*, doi: 10.1016/j.jhydrol.2009.01.043.

Huber, S., R. Fensholt, and Kjeld Rasmussen, 2011: Water availability as the driver of vegetation dynamics in the African Sahel from 1982 to 2007, *Glob. Planet. Change*, 76(3), 186-195.

Jacques, D.C., L. Kergoat, P. Hiernaux, E. Mougin, and P. Defourny, 2014: Monitoring dry vegetation masses in semi-arid areas with MODIS SWIR bands, *Remote Sens. Environ*., 153, 40–49.

Jarlan L., E. Mougin, P. L. Frison, P. Mazzega, and P. Hiernaux, 2002 : Analysis of ERS wind scatterometer time series over Sahel (Mali), *Remote Sens. Environ*., 81(2-3), 404-415.

Jarlan, L., E. Mougin, P. Mazzega, M. Schoenauer, Y. Tracol, and P. Hiernaux, 2005: Using coarse remote sensing radar observations to control the trajectory of a simple Sahelian land surface model, *Remote Sens. Environ*., 94, 269-285.

Jarlan, L., S. Mangiarotti, E. Mougin, P. Mazzega, P. Hiernaux, and V. Le Dantec, 2008: Assimilation of SPOT/VEGETATION NDVI data into a sahelian vegetation dynamics model, *Remote Sens. Environ*., 112, 1381-1394.

Jolly, W. M., and S. W. Running, 2004: Effects of precipitation and soil water potential on drought deciduous phenology in the Kalahari, *Glob. Chang. Biol*., 10, 303-308.

Karlson, M., and M. Ostwald, 2016: Remote sensing of vegetation in the Sudano-Sahelian zone: A literature review from 1975 to 2014, *J. Arid Environ*., 124, 257-269.

Kergoat, L., P. Hiernaux, C. Dardel, C. Pierre, F. Guichard, and A. Kalilou, 2015: Dry-season vegetation mass and cover fraction from SWIR1.6 and SWIR2.1 band ratio: Ground-radiometer and MODIS data in the Sahel, *Int. J. Appl. Earth Obs. Geoinf*., 39, 56-64.

Lebel, T., and A. Ali, 2009: Recent trends in the Central and Western Sahel rainfall regime (1990-2007), *J. Hydrol*., 375, 52-64.

Le Houerou, H. N., R. L. Bingham, and W. Skerbek, 1988: Relationship between the variability of primary production and the variability of annual precipitation in world arid lands, *J. Arid Environ.*, *15*(1), 1-18.

L'Hôte, Y., G. Mahé, B. Somé, and J.-P. Triboulet, 2002: Analysis of a Sahelian annual rainfall index from 1896 to 2000; the drought continues, *Hydrol. Sci. J*., 47(4), 563-572.

Lieth, H., 1975: Modeling the primary productivity of the world, In *Primary productivity of the biosphere*, 237-263, Springer Berlin Heidelberg.

Lo Seen D., E. Mougin, S. Rambal, A. Gaston, and P. Hiernaux, 1995: A regional Sahelian grassland model to be coupled with multispectral satellite data. II. Towards the control of its simulations by remotely sensed indices, *Remote Sens. Environ*., 52, 194-206.

Lotsch, A., M. A. Friedl, B. T. Anderson, and C. J. Tucker, 2003: Coupled vegetation-precipitation variability observed from satellite and climate records, *Geophys. Res. Lett.*, 30(14), doi: 10.1029/2003GL017506.

Mbow, C., R. Fensholt, K. Rasmussen, and D. Diop, 2013: Can vegetation productivity be derived from greenness in a semi-arid environment? Evidence from ground-based measurements, *J. Arid Environ*., 97, 56–65.

Meroni, M., F. Rembold, M. M. Verstraete, R. Gommes, A. Schucknecht, and G. Beye, 2014: Investigating the relationship between the interannual variability of satellite-derived vegetation phenology and a proxy of biomass production in the Sahel, *Remote Sens*., 6, 5868-5884.

Mougin, E., D. Lo Seen, S. Rambal, A. Gaston and P. Hiernaux, 1995: A regional Sahelian grassland model to be coupled with multispectral satellite data. I: Model description and validation, *Remote Sens. Environ.*, 52, 181-193.

Moulin, S., L. Kergoat, N. Viovy, and G. Dedieu, 1997: Global-scale assessment of vegetation phenology using NOAA/AVHRR satellite measurements, *J. Climate*, 10, 1154-1170.

Myneni, R. B., F. G. Hall, P. J. Sellers, and A. L. Marshak, 1995: the interpretation of spectral vegetation indexes, *Ieee T. Geosci. Remote*, 33, 481-486.

Nicholson, S. E., C. J. Tucker, and M. B. Ba, 1998: Desertification, drought and surface vegetation: an example from the West African Sahel, *Bull. Am. Meteorol. Soc*., 79(5), 815-829.

Okin, G. S., and J. Gu, 2015: The impact of atmospheric conditions and instrument noise on atmospheric correction and spectral mixture analysis of multispectral imagery, *Remote Sens. Environ*., 164, 130-141.

Olsson, L., L. Eklundh, and J. Ardö, 2005: A recent greening of the Sahel—trends, patterns and potential causes, *J. Arid Environ.*, *63*(3), 556-566.

Ozer, P., M. Erpicum, G. Demarée, and M. Vandipenbeeck, 2003: The Sahelian drought may have ended during the 1990s, *Hydrol. Sci. J.*, 48(3), 489-492.

Philippon, N., L. Jarlan, N. Martiny, P. Camberlin, and E. Mougin, 2007: Characterization of the interannual and intraseasonal variability of West African vegetation between 1982 and 2002 by means of NOAA AVHRR NDVI data, *J. Clim.*, 20, 1202-1218.

Pierre, C., G. Bergametti, B. Marticorena, E. Mougin, T. Lebel, and A. Ali, 2011: Pluriannual comparisons of satellite-based rainfall products over the Sahelian belt for seasonal vegetation modeling, *J. Geophys. Res., 116*, D18201, doi: 10.1029/2011JD016115.

Pierre, C., L. Kergoat, G. Bergametti, E. Mougin, C. Baron, M. Grippa, B. Marticorena, and M. Diawara, 2015: Modeling vegetation and wind erosion from a millet field and from a rangeland: two Sahelian case studies, *Aeol. Res.*, 19, 97-111.

Prince, S. D., 1991: Satellite remote-sensing of primary production — Comparison of results for Sahelian grasslands 1981–1988, *Int. J. Remote Sens.*, 12, 1301–1311.

Prince, S. D., D. Colstoun, E. Brown, and L. L. Kravitz, 1998: Evidence from rain-use efficiencies does not indicate extensive Sahelian desertification, *Glob. Chang. Biol.*, 4, 359-374.

Prince, S. D., K. J. Wessels, C. J. Tucker, and S. E. Nicholson, 2007: Desertification in the Sahel: a reinterpretation of a reinterpretation, *Glob. Chang. Biol.*, 13, 1308-1313.

Ramankutty, N., 2004: Croplands in West Africa: A geographically explicit dataset for use in models, *Earth Interactions*, 8, 1-22.

Roehrig, R., D. Bouniol, F. Guichard, F. Hourdin, and J. L. Redelsperger, 2013: The present and future of the West African monsoon: a process-oriented assessment of CMIP5 simulations along the AMMA transect, *J. Climate*, *26*(17), 6471-6505.

Ruppert, J. C., A. Holm, S. Miehe, E. Muldavin, H. A. Snyman, K. Wesche, and A. Linstädter, 2012: Meta-analysis of ANPP and rain-use efficiency confirms indicative value for degradation and supports non-linear response along precipitation gradients in drylands, *J. Veg. Sci.*, *23*(6), 1035-1050.

Samain, O., L. Kergoat, P. Hiernaux, F. Guichard, E. Mougin, F. Timouk, and F. Lavenu, 2008: Analysis of the in situ and MODIS albedo variability at multiple timescales in the Sahel, *J. Geophys. Res. (Atm.)*, 113, D14119, doi: 10.1029/2007JD009174

Schaaf, C., and Z. Wang, 2015: MCD43C4 MODIS / Terra+Aqua BRDF / Albedo Nadir BRDF-Adjusted Ref Daily L3 Global 0.05 Deg CMG V006, *NASA EOSDIS Land Processes DAAC*, http://doi.org/10.5067/MODIS/MCD43C4.006

Sterk, G., 2003: Causes, consequences and control of wind erosion in Sahelian Africa: a review. *Land Degrad. Dev.*, *14*(1), 95-108.

Sterk, G., L. Herrmann, and A. Bationo, 1996: Wind-blown nutrient transport and soil productivity changes in southwest Niger, *Land Degrad. Dev.*, 7(4), 325-335.

Timouk, F., L. Kergoat, E. Mougin, C. R. Lloyd, E. Ceschia, J. M. Cohard, P. de Rosnay, P. Hiernaux, V. Demarez, and C. M. Taylor, 2009: Response of surface energy balance to water regime and vegetation development in a Sahelian landscape, *J. Hydrol.*, *375*(1), 178-189.

Tracol, Y., E. Mougin, P. Hiernaux, and L. Jarlan, 2006: Testing a Sahelian grassland functioning model against herbage mass measurements, *Ecol. Model.*, 193**,** 437–446.

Traore, A. K., P. Ciais, N. Vuichard, B. Poulter, N. Viovy, M. Guimberteau, M. Jung, R. Myneni, and J. B. Fisher, 2014: Evaluation of the ORCHIDEE ecosystem model over Africa against 25 years of satellite-based water and carbon measurements, *J. Geophys. Res. Biogeosci*., 119, 1554-1575.

Tucker, C. J., C. O. Justice, and S. D. Prince, 1986: Monitoring the grasslands of the Sahel 1984–1985, *Int. J. Remote Sens*., 7, 1571–1581.

Vamborg, F. S. E., V. Brovkin, and M. Claussen, 2011: The effect of a dynamic background albedo scheme on Sahel/Sahara precipitation during the mid-Holocene, *Clim. Past*, *7*, 117-131.

Wardell, D. A., A. Reenberg, and C. Tøttrup, 2003: Historical footprints in contemporary land use systems: forest cover changes in savannah woodlands in the Sudano-Sahelian zone, *Glob. Environ. Chang.* 13, 235-254.

Zeng, N., J. D. Neelin, K. M. Lau, C. J. Tucker, 1999: Enhancement of interdecadal climate variability in the Sahel by vegetation interaction, *Science*, 286, 1537-1540.

Zhang, X., M. A. Friedl, C. B. Schaaf, A. H. Strahler, J. V. Hodges, F. Gao, B. C. Reed, and A. Huete, 2003: Monitoring vegetation phenology using MODIS, *Remote Sens. Environ.*, 84, 471-475.